Snow Particle Size Distribution From a 2-D Video Disdrometer and Radar Snowfall Estimation in East China

Ranting Tao, Kun Zhao, Hao Huang, Long Wen, Guifu Zhang, *Senior Member, IEEE*, Ang Zhou, and Haonan Chen, *Member, IEEE*

***Abstract*— In this study, as part of an effort to study snowfall characteristics and quantify winter precipitation in East China, we investigated the microphysical properties of snowfall, including size, shape, density, and terminal velocity using a 2-D video disdrometer (2-DVD) and a weighing precipitation gauge in Nanjing (NJ), East China during the winters of 2015–2019. We obtained larger snow density and terminal velocity values than those reported in the literature for this region. Higher snow density could account for higher snowflake terminal velocity, after removing the effects of observation altitude and surface temperature. We then fit the snow particle size distributions (PSDs) to the gamma model and explored the interrelationships among the model parameters and snowfall rate (SR). The relationship between radar reflectivity factor (Z_e) and SR was derived based on snow PSD measurements and the snow density relation. Using this $Z_e - \mathrm{SR}$ relationship, the estimated liquid-equivalent SRs are obtained from S-band NJ radar data collected during several snowfall events. Radar-inferred SRs showed reasonable agreement with those measured on the ground, with a mean absolute error of 16% for the collected snowfall events in NJ.**

***Index Terms*— Disdrometer, microphysical characteristics, snow, snowfall estimation, weather radar.**

I. Introduction

SNOWFALL is a common type of winter precipitation. Heavy snowfall can exacerbate city traffic and cause huge economic losses. Accurate snowfall forecasting and estimation are crucial for disaster mitigation and many other applications. However, quantitative snowfall estimation remains challenging due to the complexity and variability of snow microphysical properties. The size, terminal velocity, and density of individual snowflakes vary significantly [1], [2]. Traditionally, the liquid-equivalent snowfall rate (SR) is estimated from equivalent radar reflectivity (Z) using the $Z - \mathrm{SR}$ relationship in the form of $Z = a\mathrm{SR}^b$, where a and b are constants determined by local snowfall microphysics, such as the snow particle size distribution (PSD) [3], [4]. However, the microphysical properties of snowfall in East China remain largely unknown due to a lack of *in situ* measurements.

The 2-D video disdrometer (2-DVD) [5]–[7] is an advanced instrument that provides the most accurate measurements of liquid precipitation microphysics [8], [9]. The application of 2-DVD for solid-phase precipitation observation has increased in recent years; for example, Brandes *et al.* [10] used 2-DVD snowstorms observations to investigate the physical attributes of PSDs and derived density–snowflake size relationship for Colorado (USA), and examined the interrelationships of the parameters of gamma PSD model. Huang *et al.* [11] developed a method to derive the $Z - \mathrm{SR}$ relationship based on 2-DVD and radar measurements during the 2006–2007 winter season in Canada. In their method, the optimal values of parameterized snow density could be well estimated by minimizing the difference between 2-DVD-calculated and radar-observed reflectivity values. Adjustment for snow density was performed by Zhang *et al.* [12] for winter precipitation in Central Oklahoma, which shows promising performance in improving the simulation of radar variables from disdrometer data. Huang *et al.* [13] applied the methodology of Böhm [14] to derive mean density-size and $Z - \mathrm{SR}$ power-law relationships using a 2-DVD over Järvenpää (Finland) for snowfall events in 2010 and 2011. Nevertheless, studies performing microphysical properties and quantitative estimation of snowfall remain relatively rare, especially in China.

During the East Asia winter monsoon season, the maximum snowfall intensity usually occurs in the Yangtze–Huaihe region of East China due to abundant water vapor throughout the region [15]. Since snowfall microphysical properties vary greatly among regions with different climates, previous studies of snowfall microphysical properties in other areas may be insufficient to represent those in East China. Therefore, in this study, we investigated snowfall microphysical characteristics

Manuscript received August 10, 2019; revised January 10, 2020 and March 20, 2020; accepted April 22, 2020. Date of publication May 19, 2020; date of current version December 24, 2020. This work was supported in part by the National Key Research and Development Program of China under Grant 2017YFC1501703, in part by the National Natural Science Foundation of China under Grant 41875053 and Grant 41805025, in part by the Open Research Program of the State Key Laboratory of Severe Weather, and in part by the 5th "333 High-Level Personnel Training Project" of Jiangsu Province under Grant BRA2019037. *(Corresponding authors: Kun Zhao; Hao Huang.)*

Ranting Tao, Kun Zhao, Hao Huang, and Ang Zhou are with the School of Atmospheric Sciences, Nanjing University, Nanjing 210023, China, and also with the State Key Laboratory of Severe Weather, Joint Center for Atmospheric Radar Research of CMA/NJU, Beijing 100081, China (e-mail: zhaokun@nju.edu.cn; huanghao@nju.edu.cn).

Long Wen is with the Xichang Satellite Launch Center (XSLC), Xichang 615000, China.

Guifu Zhang is with the School of Meteorology, The University of Oklahoma, Norman, OK 73019, USA (e-mail: guzhang1@ou.edu).

Haonan Chen is with the Physical Sciences Division (PSD), NOAA Earth System Research Laboratory, Boulder, CO 80305 USA, and also with the Cooperative Institute for Research in the Atmosphere (CIRA), Fort Collins, CO 80523 USA (e-mail: haonan.chen@noaa.gov).

Color versions of one or more of the figures in this article are available online at https://ieeexplore.ieee.org.

Digital Object Identifier 10.1109/TGRS.2020.2990920

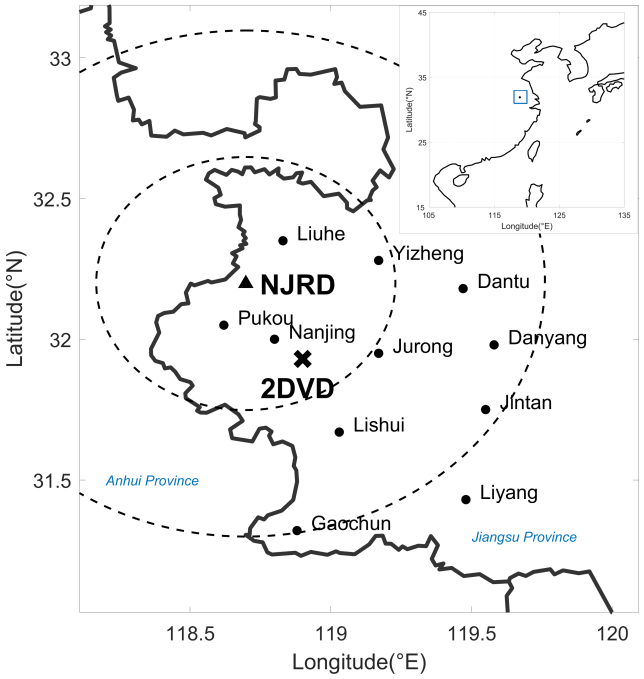

Fig. 1. Locations in East China covered by the NJRD, the 2-DVD, and 11 weighing precipitation gauges used in this study. Range rings (50-km interval) are indicated by black dashed circles. The highlighted location is in the top right corner.

based on local 2-DVD measurements obtained in Nanjing (NJ), East China, to further improve the parameterization and estimation of winter precipitation in this area. We derived and verified a radar quantitative estimation algorithm for snowfall intensity using collocated radar and snow gauge data.

The remainder of this article is organized as follows. Descriptions of the instruments used, and of the data set and analysis methodologies, are provided in Section II. Section III describes snowfall microphysical properties and the processes of liquid-equivalent snowfall estimation and verification based on the $Z - \mathrm{SR}$ relationship. The discussion and conclusions are provided in Section IV.

II. Data and Methods

A. Instrumentation

The instruments used in this study included a 2-DVD, several weighing precipitation gauges, and an S-band Doppler radar (Fig. 1). The S-band Nanjing Radar (NJRD) is deployed in NJ, Jiangsu Province (32.19°N, 118.69°E) at an altitude of about 138.2-m a.s.l. The 2DVD is deployed at the Jiangning (JN) national weather station (31.93°N, 118.90°E; ∼35.2-m a.s.l.). JN station is approximately 35 km from NJRD. The weighing precipitation gauges used in this study are all located within 100 km of NJRD; one is collocated with 2-DVD at JN station as shown in Fig. 2 (distance ∼ of about 20 m).

The 2-DVD is the third-generation version produced by JOANNEUM RESEARCH (Graz, Austria). The 2-DVD includes two orthogonal high-speed line-scan cameras with a height offset of 6–7 mm. Particles passing through the approximately 10 cm × 10 cm virtual measuring area, formed

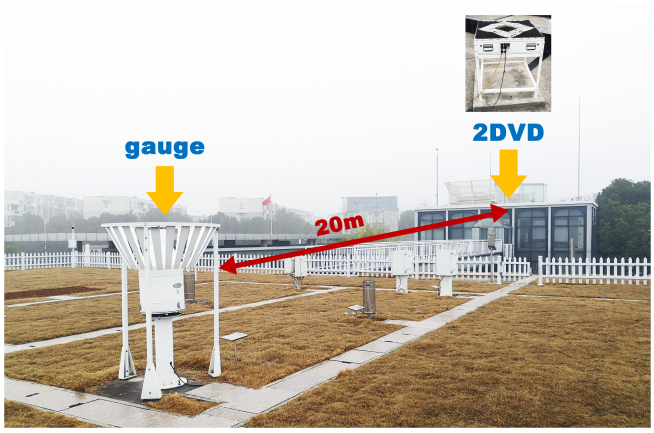

Fig. 2. Relative positions of the 2-DVD and the weighing precipitation gauge at JN station.

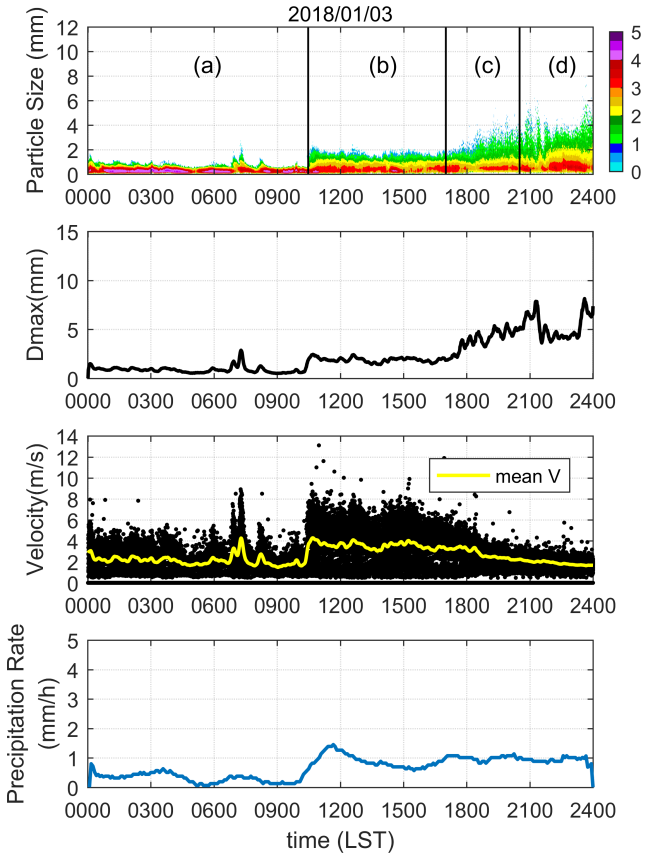

Fig. 3. Time series of the PSD, maximum diameter ($D_{\max}$), terminal velocity, and precipitation rate for the event on January 03, 2018. Colors in the PSD time-series indicate particle number concentrations after logarithmic transformation.

by the cross section of the two optical paths, obstruct light and cast shape shadows on the cameras [6]. The 2-DVD obtains a pair of pictures of each particle, along with volume, equivolumetric diameter, and terminal velocity data. Further information about instrument capability is available on the manufacturer website (www.distrometer.at).

The weighing precipitation gauges used in this study are all installed at automatic meteorological network stations in East China (black dots in Fig. 1), operated by the China Meteorological Administration (CMA). The gauge has an

TABLE I
SNOWFALL EVENTS MEASURED BY 2-DVD FROM 2015 TO 2019

Year	Case	Snow Period (LST)	T (°C)	T_w (°C)	Wind speed (m/s)	Classification by terminal velocity
2015	1	01:36-08:00 28 Jan	-0.56	-1.4	3.1	low
		21:00-24:00 28 Jan	0.4	0.0	3.0	low
		11:50-18:00 29 Jan	0.41	0.0	2.8	low
2016	2	19:30-24:00 20 Jan	-0.06	-1.4	2.4	low
		00:00-08:00 21 Jan	-0.71	-1.6	1.8	low
		09:00-24:00 22 Jan	0.41	-0.6	3.4	high
	3	13:00-21:00 31 Jan	-0.57	-1.6	3.2	high
	4	11:00-18:00 23 Nov	0.45	-0.2	3.3	high
2018	5	00:00-24:00 04 Jan	0.41	0.0	2.4	high
	6	13:00-17:00 09 Dec	0.97	-0.2	2.4	low
	7	13:00-21:00 30 Dec	-1.4	-2.6	2.5	high
2019	8	02:00-15:00 09 Jan	0.51	0.0	1.6	high

T is the mean surface temperature obtained from Stevenson screen at JN station. T_w is the mean wet-bulb temperature calculated from surface temperature and relative humidity [21]. Two categories of the snowfall events classified by terminal velocity are described with high terminal velocity and low terminal velocity.

TABLE II
TERMINAL VELOCITY RELATIONS IN PREVIOUS STUDIES AND THIS STUDY

Study	Relation	Snow Type
Brandes (2002) [22]	$v_t = -0.1021 + 4.932D - 0.9551D^2 + 0.07934D^3 - 0.002362D^4$	Rain
Jeong-Eun (2015) [23]	$v = 1.03D^{0.71}$	Needle
Locatelli and Hobbs (1974) [24]	$v = 1.3D^{0.66}$	Lump graupel
	$v = 0.79D^{0.27}$	Densely rimed aggregates
	$v = 0.81D^{0.16}$	Unrimed aggregates
This study	$v = 1.03D^{0.25}$	low terminal velocity cases
	$v = 1.29D^{0.29}$	high terminal velocity cases

orifice diameter of 20 cm. It records the liquid-equivalent accumulated height of snow at 1-min intervals (0.1-mm resolution). Wind speed is the most important factor determining gauge catch efficiency [15]. The snowfall events analyzed in this study had ambient wind speeds of <3.5 m/s (Table I). In order to make the snow gauge measurements more accurate, we performed wind-loss corrections of snow gauge data according to the equation described in [20]. They compared the gauge measurements of snowfall with and without the Double Fence Intercomparison Reference (DFIR) shield which is an international standard reference windshield used by the World Meteorological Organization for accurate snow gauge measurements [16], [17]. Then, the snow gauge catch ratio R (Gauge/DFIR) is parameterized by wind speed W_s as follows:

$$R = \exp\left(4.605 - 0.06 * W_s^{1.4}\right).$$

Finally, the snow gauge catch ratio is used for the correction of snow gauge measurements in our study.

NJRD is operated in volume coverage pattern (VCP) mode 21, which includes nine elevation angles (0.5°, 1.5°, 2.4°, 3.3°, 4.3°, 6.0°, 9.9°, 14.6°, and 19.5°). The temporal resolution of NJRD is about 6 min; the gate spacing and azimuth resolution are 0.25 km and 1°, respectively. In this study, we used NJRD data at the 0.5° PPI scans within an area average of 1 km × 1 km aloft the instruments for comparison.

B. Data Set

From January 2015 to February 2019, eight snowfall events in the observation region were recorded (Table I). Some of these events were split into multiple time periods. To ensure collection of sufficient snowflake samples, 2-DVD and weighing precipitation gauge data were integrated at 5-min intervals.

As shown in Table I, the surface wet-bulb temperatures T_w during the snowfall events were ≤0 °C, indicating the hydrometeors were dry snow [18]–[21]. Liquid and mixed-phase precipitation data recorded at the JN site were excluded from the analysis. To illustrate the process of snowfall period selection, Fig. 3 shows a time series of the snowfall characteristics for a rain–snow transition event (January 03, 2018), including snow PSD, maximum diameter (D_{max}), terminal velocity, and precipitation rate, as measured by the 2-DVD and weighing precipitation gauge. The terminal velocity data for each precipitation period are presented in Fig. 4. The representative terminal velocity relationships of different particle types are also shown for comparison (Table II) [22]–[24]. Period (a) was characterized by light rain with D_{max} seldom exceeding 2 mm (Fig. 3) and the particle terminal velocity matching well with the relation for rain [22] [Fig. 4(a)]. An increase in precipitation rate during the moderate rain period (b) corresponded to increases in D_{max} and terminal velocity. During the transition from rain to snow in period (c), D_{max} increased and the terminal velocity decreased. The particle velocities during this mixed-phase precipitation period were between those of rain and snow [Fig. 4(c)]. During the pure snowfall period (d), D_{max} exceeded 8 mm and the terminal velocity was $<3\ m \cdot s^{-1}$; no significant increase in terminal velocity was noted when particle size

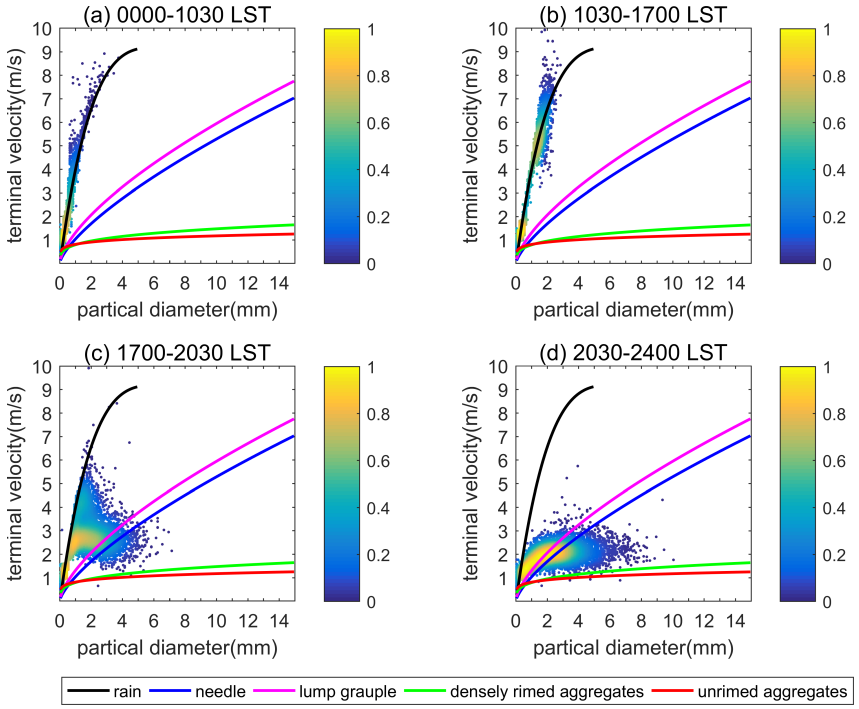

Fig. 4. Terminal velocity versus diameter for periods of (a) light rain, (b) moderate rain, (c) mixed-phased precipitation, and (d) snow on January 03, 2018, obtained via the 2-DVD. Colors denote scatter density. Curves are the representative relationships of different particle types (Table II).

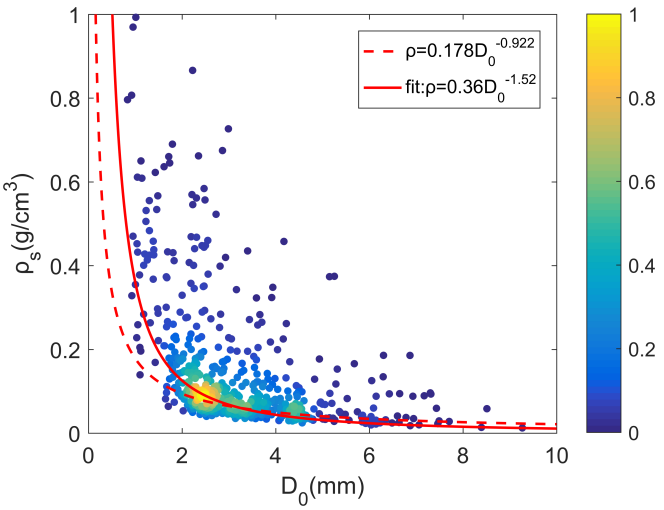

Fig. 5. Snow density–diameter relationship derived from the 2-DVD measurements and weighing precipitation gauge data obtained during the snowfall events listed in Table I. Colors denote scatter density. The relationship derived in this study and by Brandes *et al.* [10] is indicated by red solid and dashed lines, respectively.

increased [Fig. 4(d)]. Due to the short snowfall period on January 03, 2018, we included snow data from the following day (January 04, 2018; a whole-day snowfall event) in the analysis.

C. Snow PSD

We sorted 2-DVD-observed snowfall particles from 0.1 to 15 mm into 150 size bins (0.1-mm intervals). The snow PSD is expressed by

$$N(D_i) = \frac{1}{\Delta t * \Delta D} \sum_{j=1}^{n_i} \frac{1}{A_j * v_j} \tag{1}$$

where D_i (mm) and $N(D_i)$ (mm^{-1} · m^{-3}) are the mean diameter and mean number concentration of particles in class i, Δt (s) is the time interval, ΔD (mm) is the particle size class width, and A_j (m^2) and v_j (m·s^{-1}) are the effective measuring area and terminal velocity of particle j, respectively. Due to the complexity of snowflake shapes, 2-DVD mismatching can occur. We filtered initially matched particles using the method of Bukovčić *et al.* [25]. The products of the height ratio of the orthogonal images and the ratio of measured terminal velocity to the predetermined value are calculated for the match samples. The samples with the product below the threshold value of 0.5 are filtered out. Note that, filtered mismatching particles can cause errors in measured PSD. Accordingly, filtered PSD $N_m(D_i)$ was corrected following the method of Huang *et al.* [13] using adjustment factor γ, which is derived as follows γ, as shown at the bottom of the next page, where 0.4 (100/250) is the ratio of the theoretical number of snowflakes in the virtual measuring area and the theoretical number of snowflakes in the scan area of a single camera. The $N_m(D_i)$ for the 2-DVD measurements is then readjusted to $N(D_i) = \gamma * N_m(D_i)$.

The total number concentration of particles N_T (m^{-3}) is given by

$$N_T = \int_{D_{\min}}^{D_{\max}} N(D) dD. \tag{2}$$

The well-known three-parameter gamma model is widely used to describe the size distribution of raindrops [26], ice particles and cloud droplets [27], [28], and snow particles [29]–[31], as follows:

$$N(D) = N_0 D^{\mu} \exp(-\Lambda D) \tag{3}$$

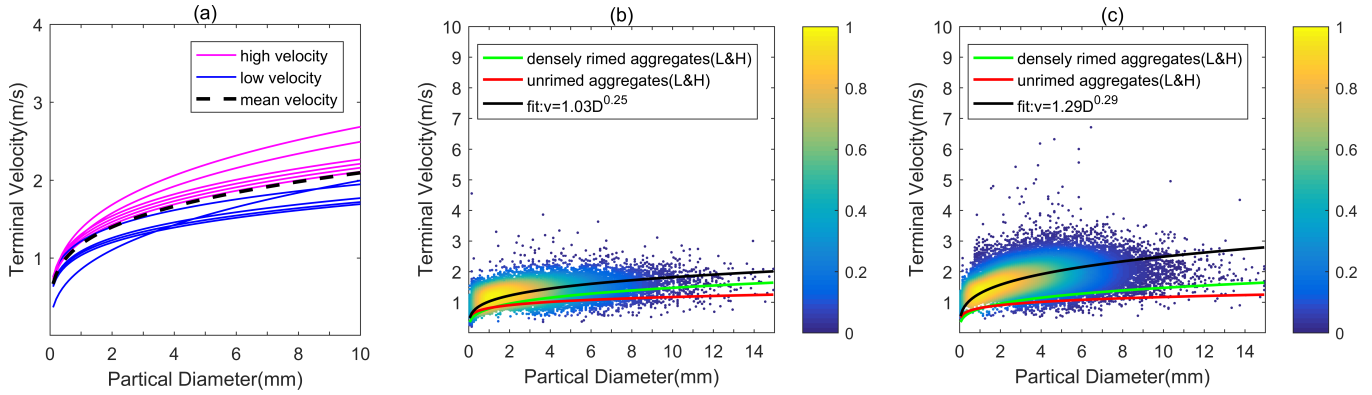

Fig. 6. (a) Low and high terminal velocity snowfall events, indicated by blue and pink lines, respectively. The black dashed line indicates the mean terminal velocity among all cases. (b) Scatterplots of terminal velocity versus particle diameter for low terminal velocity snowfall events. Black lines are power-law fitting curves. (c) Scatterplots of terminal velocity versus diameter for high terminal velocity snowfall events. Black lines are power-law fitting curves. Colors in (b) and (c) denote scatter density. Green and red lines in (b) and (c) are the terminal velocity relationships summarized in Table II.

where N_0 ($\text{mm}^{-\mu-1}\cdot\text{m}^{-3}$), μ (dimensionless), and Λ (mm^{-1}) are the intercept, shape, and slope parameters, respectively. The M246 (the 2nd, 4th, and 6th moments of the observed particle distribution) truncated-moment method was used to calculate the three parameters [32].

D. Parameterization of Snow Density

In previous studies, snow density (ρ_s) was parameterized using numerous diameter variables, including the median volume diameter (D_0) [10], geometric mean of the major and minor axes of particles [33], minimum circumscribed circle of the particle projected area [28], and the equivalent volume diameter [34]. In this study, we used D_0 to derive the power-law $\rho_s - D_0$ relationship, similar to the method used by Brandes *et al.* [10] but from a weighing precipitation gauge instead of a heated tipping-bucket gauge. Snow density was calculated using a gravimetric measurement method, as follows:

$$\rho_s = \frac{m_{\text{snow}}}{V_{\text{snow}}} \tag{4}$$

where m_{snow} and V_{snow} represent the mass and volume, respectively, of snow deposited during a 5-min period. Snow mass per unit area can be expressed as

$$m_{\text{snow}} = \rho_w h \tag{5}$$

where ρ_w ($\text{g}\cdot\text{cm}^{-3}$) is the density of water and h (mm) is the liquid-equivalent accumulated height of snow measured by the weighing precipitation gauge. We then estimated the snow volume per unit area as

$$V_{\text{snow}} = \frac{\pi}{6}\int D^3 V_t N(D) dD \tag{6}$$

using the 2-DVD-measured terminal velocity (V_t) and the number concentration of particles, i.e., $N(D)$. It should be noted that sampling differences between the weighing precipitation gauge and 2-DVD are likely to limit the accuracy of snow density calculations.

The median volume diameter D_0 is defined as

$$\int_{D_{\min}}^{D_0} D^3 N(D) dD = \int_{D_0}^{D_{\max}} D^3 N(D) dD \tag{7}$$

where the minimum diameter ($D_{\min}$) and $D_{\max}$ are obtained from the 2-DVD measurements. The relationship between density ρ_s and D_0 is thus established. In this study, power-law relationships were derived using the weighted total least squares (WTLS) fitting technique [35].

E. Quantitative Estimation of Snow

Based on the snow density–diameter relationship, radar reflectivity can be calculated directly from measured PSDs using the Rayleigh-scattering approximation for low density, irregularly shaped dry snow particles [36]. The dielectric constant of snowflakes $|K_s|$ determined using the Maxwell Garnett mixing formula for a mixture of ice and air is given as $|K_s|^2 = (\rho_s^2/\rho_i^2)|K_i|^2$ [37]. The equivalent radar reflectivity factor Z_e for snowflakes can be written as [38]

$$Z_e = \frac{|K_i|^2}{\rho_i^2 |K_w|^2}\int_{D_{\min}}^{D_{\max}} \rho_s^2 D^6 N(D) dD \tag{8}$$

where $|K_i| = ((\varepsilon_i - 1)/(\varepsilon_i + 2))$, ε_i is the relative dielectric constant of ice, $|K_w| = ((\varepsilon_w - 1)/(\varepsilon_w + 2))$, and ε_w is the relative dielectric constant of water. The density of ice is $\rho_i = 0.917\ \text{g}\cdot\text{cm}^{-3}$ [39].

The observed PSDs, particle terminal velocity V_t, and $\rho_s(D)$ were then combined to calculate melted liquid-equivalent SR (in $\text{mm}\cdot\text{h}^{-1}$),

$$\text{SR} = \frac{\pi}{6}\int \rho_s(D) D^3 V_t N(D) dD. \tag{9}$$

Based on measured snow PSD for all events analyzed in this study, the $Z_e - \text{SR}$ relationship can be derived from (8) and (9) using the WTLS fitting method.

$$\gamma = 0.4 * \frac{\#\text{ of snowflakes actually counted in scan area of a single camera}}{\#\text{ of matched snowflakes in virtual measuring area}}$$

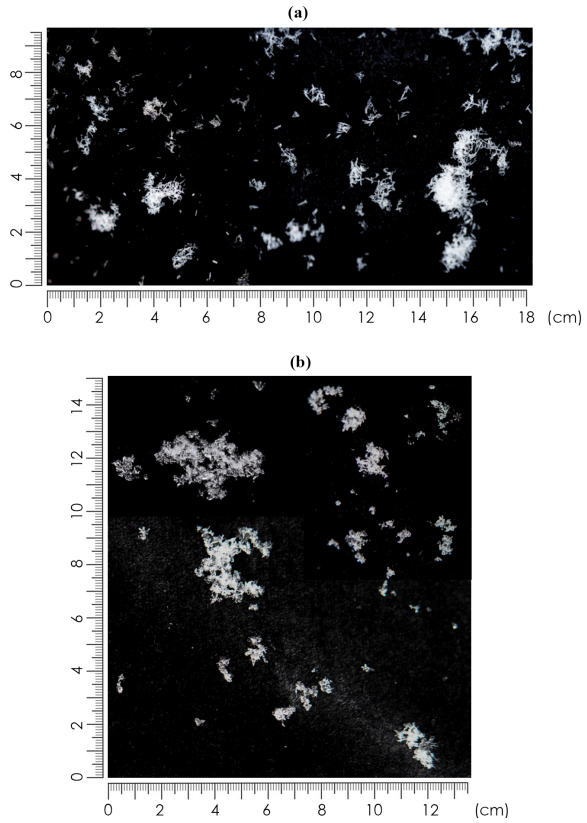

Fig. 7. (a) Aggregates of needles at 16:05 LST on December 09, 2018 (Case 6 in the low terminal velocity group) and (b) aggregates of dendrites and plates at 14:34 LST on January 09, 2019 (Case 8 in the high terminal velocity group).

III. Results

A. Snow Density and Terminal Velocity

Snow density differs among climate regions. We derived the $\rho_s - D_0$ relationship for snowfall events in this study to optimize the estimation of radar reflectivity factor and SR. A total of 600 valid density data points for eight events are shown in Fig. 5. The relatively diffuse pattern of data points (scatter density < 0.1) may have been caused by the variation in the type of snowflakes and riming degree among events, or by observation errors. The fit $\rho_s - D_0$ relationship (red solid line) is expressed as follows:

$$\rho_s = 0.36 D_0^{-1.52}. \tag{10}$$

The coefficient of the relationship was larger (0.36), and the negative exponent was smaller (-1.52), in this study versus Brandes *et al.* [10] (red dashed line; coefficient, 0.178; exponent, -0.922). Snow density was higher when $D_0 < 3.2$, and was close to that of Brandes *et al.* [10] when $D_0 > 3.2$ (Fig. 5), probably due to the degree of looseness and riming, and the content of ice. Differences among observation instruments and data processing procedures may also cause differences in the derived relationships.

The terminal velocity–diameter relationship is in the form of $v = aD^b$. All snowfall events were divided into two categories (Table I) according to the comparison between the terminal velocities in each case and the mean terminal velocity of all cases. Snowfall events with the terminal velocities

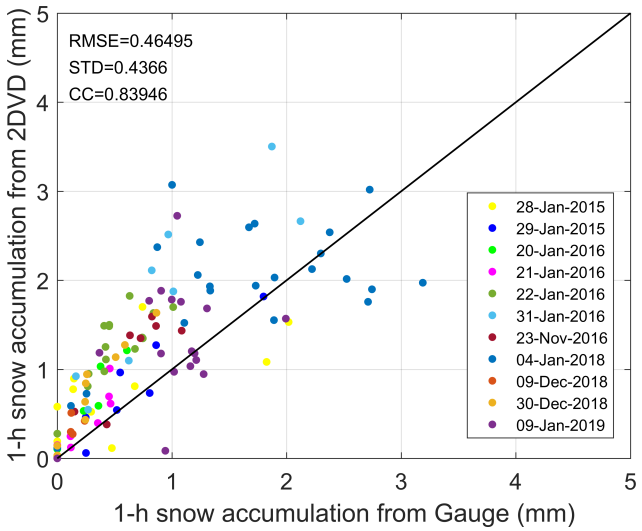

Fig. 8. Scatterplot of 1-h liquid-equivalent snow accumulation estimated from 2-DVD and snow gauge data.

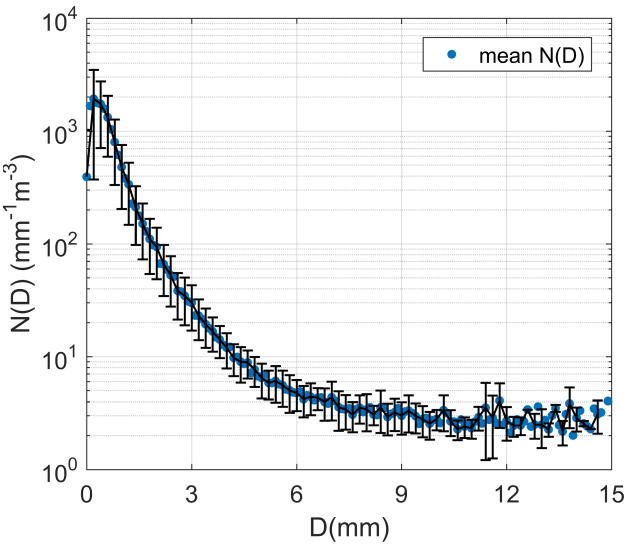

Fig. 9. Mean PSD of eight snowfall events determined by the 2-DVD. Blue dots indicate averaged $N(D)$ for all size ranges; standard deviations are indicated by vertical bars.

higher (lower) than the mean terminal velocity were classified into the high (low) terminal velocity group, shown as pink (blue) lines in Fig. 6(a). Splitting the snowfall events into two categories improved the fit (Fig. 6); otherwise high terminal velocity values would mask lower values. For comparison, we also show the relationships proposed by Locatelli and Hobbs [24], which have been applied extensively for solid precipitation (Fig. 6 and Table II). In five of eight cases (Cases 3, 4, 5, 7, and 8) and a part of Case 2 (09:00–24:00, January 22, 2016), particles had a relatively higher terminal velocity [1–3 m $\cdot$ s^{-1}; Fig. 6(c)] with larger spectral width. Terminal velocities were lower in the other periods and were within a narrower range [0.8–2 m $\cdot$ s^{-1}; Fig. 6(b)]. The $v - D$ curve of lower terminal velocity group was closer to, but still higher than, that for densely rimed aggregates described by Locatelli and Hobbs [24]. Similar to those described by Barthazy and Schefold [40], the mean terminal velocity of

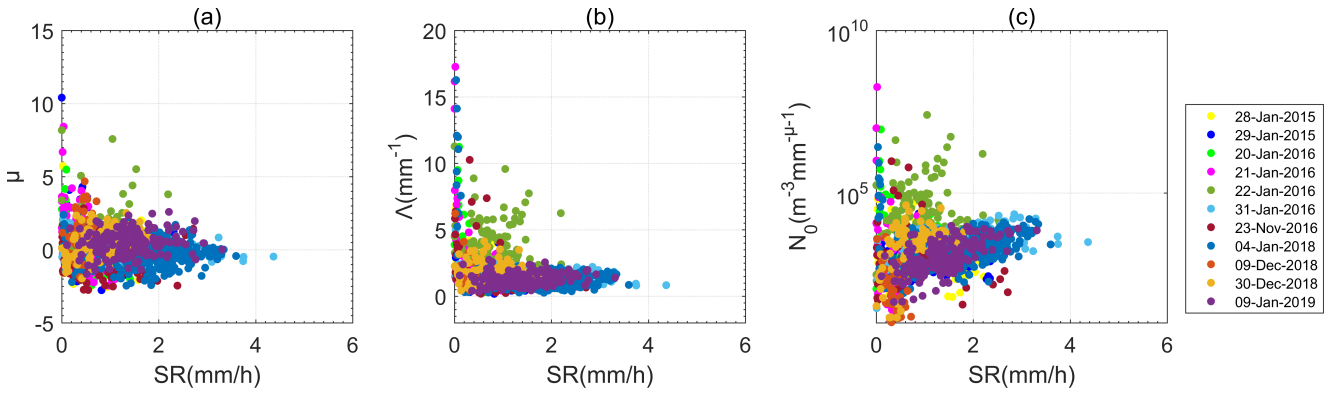

Fig. 10. (a) Shape parameter μ, (b) slope parameter Λ, and (c) concentration parameter N_0 of the gamma PSD model versus SR for all snowfall periods.

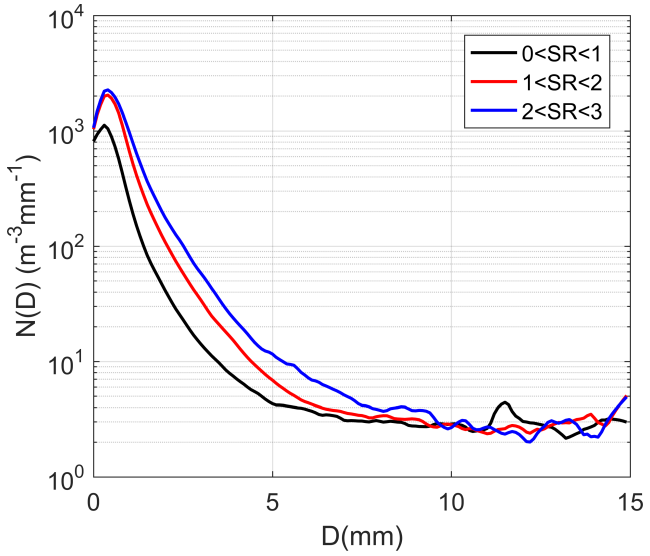

Fig. 11. Mean PSDs for three SR ranges ($0 < SR < 1$, $1 < SR < 2$, and $2 < SR < 3$) based on the 2-DVD measurements.

snowflakes in this study was higher than that for aggregates of Locatelli and Hobbs [24]. Because measurement elevation was similar between these two studies (750–1500-m a.s.l. in [40]; 1604-m a.s.l. in [24]), the atmospheric pressure difference was excluded from the interpretations of the higher observed terminal velocities in their study. However, our measurements were obtained at 42.2-m a.s.l. For a given ice crystal diameter, terminal velocity was lower at high pressure than at low pressure [41]. The higher snowfall terminal velocities in our study were not caused by differences in observation altitude.

Brandes *et al.* [5] showed that the terminal velocity of snowflakes in eastern Colorado was close to that reported by Locatelli and Hobbs [24] for densely rimed aggregates at temperatures near -1 °C ($-2 < T < 0$ °C); they also found that the terminal velocity of the aggregates increased with ground temperature. In this study, all events occurred within a narrow temperature range close to 0 °C (Table I). There was no monotonic correlation between terminal velocity and ground temperature in our study, indicating that the higher terminal velocity of the snow aggregates was not closely related to ground temperature.

To further explore the factors affecting snowflake terminal velocity, it is necessary to identify the type of formed aggregates. The images of predominant crystal types were captured during two snowfall events, i.e., Case 6 (in the low terminal velocity group) and Case 8 (in the high terminal velocity group) (Fig. 7). These images were taken using a high resolution digital single-lens reflex camera after collecting snowflakes on black velvet. Snowflakes in Case 6 were almost exclusively aggregates of needles with low terminal velocity, whereas those in Case 8 consisted of a mixture of plates and dendrites with high terminal velocity. Thus, it is possible to infer that the wider range of velocities observed in Case 6 than that in Case 8 was caused by the diversity in snowflake types. The photographs showed that the snowflakes in Case 8 were formed by ice crystals aggregation; this higher ice content increased the terminal velocity of Case 8 snowflakes relative to those of Case 6. This may suggest that different snowflake types in each event result in two different terminal velocity categories in this study. Plates or dendrites occur at lower temperatures (-8 °C to -22 °C) than needles (0 °C to -8 °C), as shown in the habit diagram presented by Bailey and Hallett [42]. Hence, differences in upper ambient temperature and ice supersaturation among snowfall cases may have led to the formation of different snowflake types.

We observed larger snow density values in this study ($D_0 < 3.2$) than reported previously in the literature, which suggests that the density of the snowflakes may be responsible for the higher terminal velocities in this study.

B. Statistical Characteristics of Snow PSD

The 1-h liquid-equivalent snow accumulation data for all snowfall events, as estimated based on 2-DVD and measured by the weighing precipitation gauge, are presented in Fig. 8. The standard deviation was 0.44 mm and the correlation coefficient was 0.84. Generally, the 2-DVD observations showed reasonably good agreement with the gauge data, indicating the reliability of the 2-DVD data for calculating SR.

It is possible to specify a general form of snow PSD since snow data behave much more consistently than rain data on a single day [43]. The mean PSD of eight snowfall events obtained from the 2-DVD is shown in Fig. 9. The peak concentration (diameter $\sim$ 0.3 mm) was comparable to that of the stratiform rain in NJ [44]. Compared to snowfall

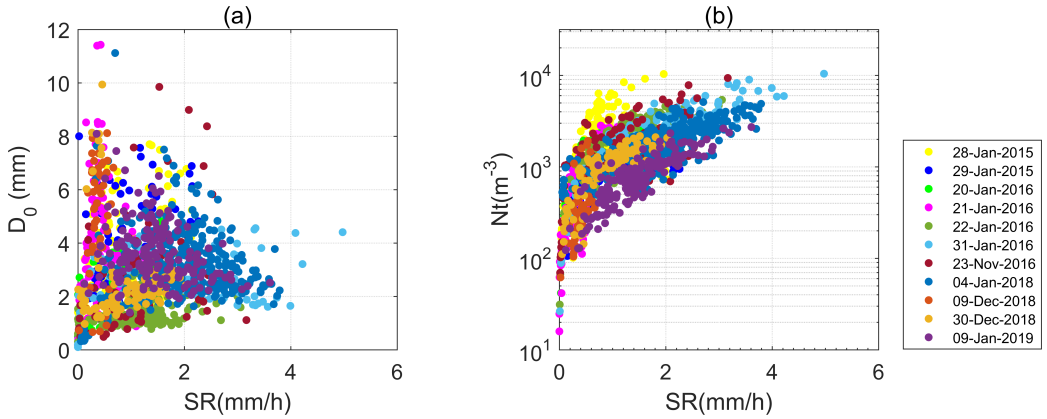

Fig. 12. (a) Median volume diameter (D_0) and (b) total number of particles (N_t) versus SR for all snowfall periods.

TABLE III
INTERRELATIONSHIPS AMONG THE THREE PARAMETERS AND SR

Parameters-*SR* / *SR*	μ-*SR*	Λ-*SR*	N_0-*SR*
SR<1.5 mm/h	small variability in μ	large variability in Λ	large variability in N_0
SR>1.5 mm/h	tend to converge with increasing *SR* and distributed around 0	tend to be consistent and concentrated at 0 – 2 mm^{-1}	tend to converge with an increasing trend

PSDs obtained in Finland [13] and Colorado [10], the snow particle size corresponding to the maximum concentration is smaller in this study. Another difference is shown by the steeper curve when $D > 1$ mm, which characterized with lower concentrations for larger particle sizes. This may be attributed to occasional collisions and coalescence of small particles during the particle growth process. We also found that the curve describing the mean PSD tended to flatten out at large particle sizes ($D > 8$ mm) as the result of PSD averaging, where the PSD diameter range varied over time. Similar particle concentrations in the tail of the mean distribution suggest that the concentrations of the aggregates reached equilibrium within 1–4 $mm^{-1} \cdot m^{-3}$ when $D > 8$ mm.

Three governing parameters of gamma PSD were derived for particles ranging from 0.1 to 15 mm in diameter using the truncated moment fitting method. As shown in Fig. 10(a), values of the shape parameter μ are distributed around 0, with 53.45% and 46.55% positive and negative values, respectively. Fluctuations in μ above and below 0 indicate considerable variability in the shape of the PSD at small sizes. Negative μ values are common for ice particle distributions in clouds [27]. In comparison, 21% of the μ values were negative for the snowstorms described by Brandes *et al.* [10]. Large variability in the slope parameter Λ occurred at SR < 1.5 mm/h [Fig. 10(b)]; Λ values tend to be consistent and concentrated at 0–2 mm^{-1} when SR > 1.5 mm/h. N_0 values varied by more than two orders of magnitude when SR < 1.5 mm/h, and tended to converge at high SRs (>1.5 mm/h) with an increasing trend. This result is opposite to that reported by Brandes *et al.* [10], where N_0 showed a negative relationship with SR. Generally, when SR > 1.5, both μ and Λ converged to near-constant values, whereas N_0 increased significantly with SR. The increase of N_0 with SR reflects an increase in the entire PSD curve as SR increases. Mean PSDs for different SR ranges are shown in Fig. 11. To reduce the effect of sampling error, we applied the low-pass filter method with a five-point window. Higher SRs were associated with higher concentrations of particles with diameter < 10 mm. The large magnitude and variation of and N_0 when SR < 1.5 are mainly attributed to snowfall periods of Case 2 and Case 7 (January 22, 2016 and December 30, 2018). These two snowfall periods were characterized by small D_0 and high N_t values (Fig. 12), indicating narrower PSDs and the dominant of small particles. Interrelationships among the three governing parameters and SR are summarized in Table III.

Scatterplots of $D_0 - \mathrm{SR}$ and $N_t - \mathrm{SR}$, based on disdrometer data of the eight events, are shown in Fig. 12 and reveal the contributions of particle diameter and concentration to snow intensity. Generally, both D_0 and N_t tended to increase with SR, but increased slowly at high SRs. The snowfall periods of Cases 2 and 6 (January 21, 2016 and December 09, 2018) had small and nearly constant SRs, with highly variable D_0 and N_t. For the snowfall periods of Case 2 and 7 (January 22, 2016 and December 30, 2018), the D_0 values were small and varied slightly as SRs increased; N_t was relatively high and increased markedly with SR compared to the other cases. This suggests that the main factor contributing to the increase in snowfall intensity during these two snowfall periods was the increase in particle number concentration. During all other events, increased SRs contributed to both particle diameter and concentration. This analysis is summarized in Table IV.

C. Snowfall Estimation

The agreement between disdrometer-based radar reflectivity and the radar-measured result can be used to verify the reliability for 2-DVD-derived snowfall estimation. Fig. 13(a) compares the time series of Z_e obtained from disdrometer data and

TABLE IV
CONTRIBUTIONS OF D_0 AND N_t TO SR

Snow events \ Parameters	D_0	N_t	Analysis
21-Jan-2016 09-Dec-2018			small and nearly constant *SR*s with highly variable D_0 and N_t——excluded from the analysis
22-Jan-2016 30-Dec-2018	–	+	small D_0 and varied slightly as *SR*s increased, while N_t is relatively high and increases markedly with *SR*——increased *SR* is mainly contributed to N_t
other events	+	+	Both D_0 and N_t increase with SR——increased *SR* is contributed to both D_0 and N_t

In the table, + indicates dominant contributor and – indicates lesser contributor to snow intensity.

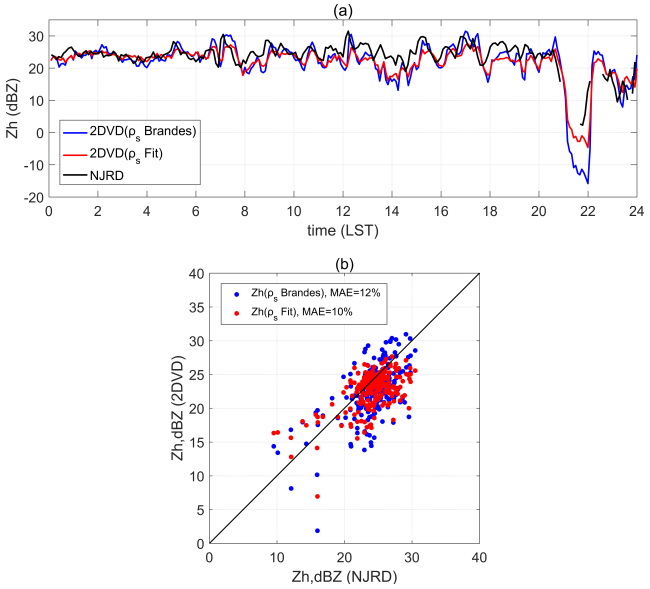

Fig. 13. (a) Time series and (b) scatterplot comparing reflectivity values obtained from NJRD measurements and 2-DVD calculations with derived snow density and reference snow density for Case 5 (January 04, 2018).

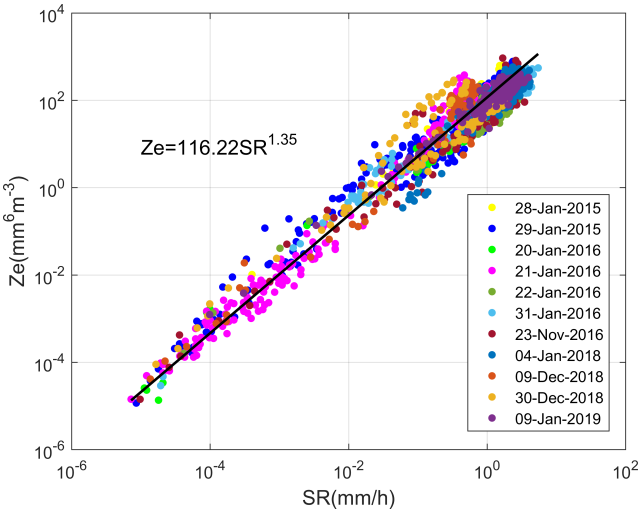

Fig. 14. Scatterplot of the equivalent radar reflectivity factor (Z_e) versus SR based on the 2-DVD data for all snowfall periods. The solid line is the line of best fit.

NJRD-measured radar reflectivity data over JN station (area average of 1 km × 1 km, elevation angle of 0.5°) for Case 5 (January 04, 2018), when snowfall persisted for almost the entire day, before gradually decreasing after 21:00 LST. The radar reflectivity calculations used snow density relationship from Brandes *et al.* [10] and that from this study are compared to the radar measurements. There were missing data among the radar measurements for the periods 21:00–21:40 LST and 22:20–22:40 LST. Considering the differences in sampling volume and observation height between the two instruments, the measured and derived reflectivity values show good overall agreement. As shown in Fig. 13(b), overestimations of large values and underestimations of small values were improved for Case 5 (January 04, 2018) by using the snow density-size relationship derived in this study instead of the snow density of Brandes *et al.* [10]. The mean absolute error (MAE) of radar reflectivity retrieval, based on the derived snow density relationship, was 10%, compared to 12% based on snow density relationship from Brandes *et al.* [10]. For all snowfall events collected, the average of MAE was 21.9% and 17.1% using ρ_s from Brandes *et al.* [10] and this study, respectively.

The 2-DVD derived Z_e and SR pairs for all eight snowfall events are presented in Fig. 14. The relation constructed by WTLS method is

$$Z_e = 116.22\mathrm{SR}^{1.35}. \tag{11}$$

To evaluate the performance of radar-based estimations, we examined the MAE of snowfall estimates for the cases. The average MAE between radar-based snow estimates and snow gauge data was 16% among all snowfall events in NJ. Case 5 (January 04, 2018), i.e., the whole-day snowfall event, showed the most accurate estimation. Ground-based verification of a 21-h snowfall accumulation period, estimated by NJRD for Case 5 (January 04, 2018) using the newly derived $Z_e - \mathrm{SR}$ relationship, is shown in Fig. 15. The lowest radar beams in the sector between 100° and 130° were partially blocked by terrain at the Danyang, Jurong, and Jintan stations. Radar reflectivity in areas where beams are blocked result in underestimation of snowfall. To avoid any effects of radar beam blockage, snowfall estimations from these three gauge stations were excluded from the analysis. The peak snow accumulation > 50 mm (Fig. 15) occurred within an area about 40 km from the radar. Overall, radar-derived accumulation data showed reasonable agreement with the gauge data.

For a more detailed comparison, hourly liquid-equivalent snowfall accumulation data, derived from radar and gauges for five sites around JN for Case 5 (January 04, 2018), are shown

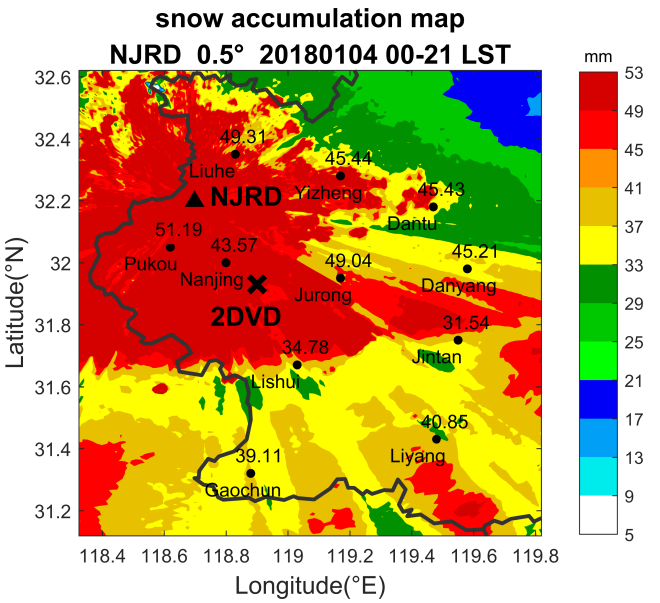

Fig. 15. Map of a 21-h period of snowfall accumulation for Case 5 (January 04, 2018) derived based on $Z_e - \mathrm{SR}$ relationship. Black solid triangle and black cross indicate the locations of NJRD and the 2-DVD, respectively. Black solid dots indicate snow gauge locations; values above these dots denote liquid-equivalent snow accumulation (mm).

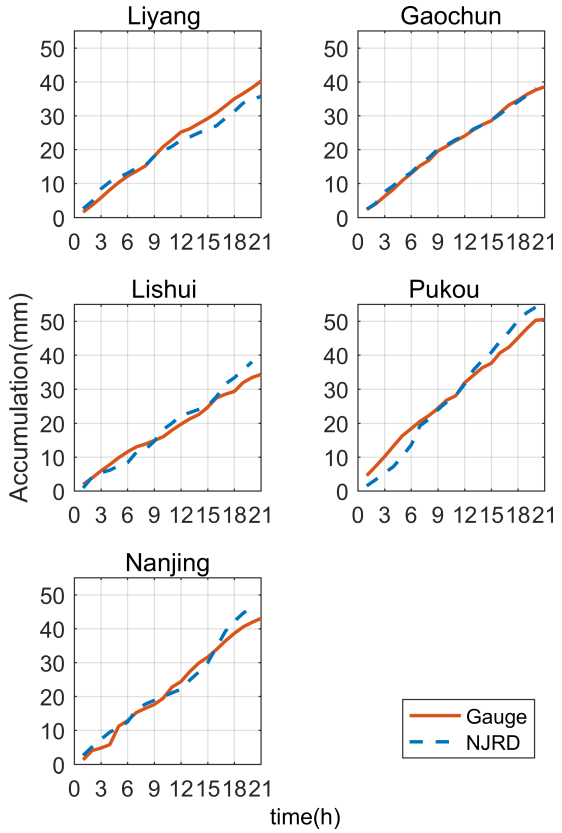

Fig. 16. Comparison of hourly liquid-equivalent snow accumulation data obtained from NJRD and weighing precipitation gauge at five sites near JN for Case 5 (January 04, 2018).

in Fig. 16. The overall agreement was reasonable overall, with an estimated MAE of 15% for all five sites, among which the radar-based snow estimates at Gaochun were the most accurate (MAE, 4%).

IV. Conclusion and Discussion

In this study, radar and disdrometer data collected during the winters of 2015–2019 were analyzed to resolve the microphysical properties (density and terminal velocity) of snowfall and PSD characteristics and to derive a radar-based snowfall estimation algorithm for East China. Combining data sets from the 2-DVD and weighing precipitation gauges, we developed a snow density-size relationship. Compared to the result reported by Brandes *et al.* [10], mean snow density was greater in this study when $D_0 < 3.2$ mm. We derived $v - D$ relationships for two categories of snowflake terminal velocity (Table II). The differences in the terminal velocity between two types of events may be explained by differences in snowflake types. The terminal velocities of aggregates in both categories were higher than the reference terminal velocity relationships. After examining several variables that could influence the terminal velocities, such as surface temperature and observation altitude, we concluded that higher snowflake terminal velocity was mainly caused by higher snow density.

Snow PSDs were fit to the gamma model with three governing parameters, and the interrelationships among those parameters in terms of SR were described. The results showed no clear relationship between SR and the three parameters when SR < 1.5 mm/h. However, when SR > 1.5 mm/h, both μ and Λ tended to converge, and N_0 showed an increasing trend with SR. These results indicate that the snow particle concentration increased as SR increased. We then evaluated the contribution of particle diameter and total number concentration to snowfall intensity. The microphysical characteristics differed among the snowfall cases. The increase in SR was influenced by both the diameter and concentration of snow particles.

The $\rho_s - D_0$ relationship derived in this study performed better than that derived previously in the calculation of radar reflectivity, indicating that (10) well represents the snow density for the snowfall events in NJ. This density–size relationship can be used to calculate radar reflectivity and SR, and the $Z_e - \mathrm{SR}$ power-law relationship can be then derived. To quantitatively validate the radar-derived snowfall estimation, we used Case 5 (January 04, 2018) as an example. The average MAE among the snowfall events in NJ was 16%, indicating good agreement between radar-inferred and ground-measured liquid-equivalent accumulation data. Although the localized $Z_e - \mathrm{SR}$ relationship is reasonably accurate as a basis for snowfall estimation around NJ, this relationship should be applied with caution for the whole area covered by the radar because it was derived from a limited region, i.e., that where *in situ* observations are available.

This study documents the basic microphysical characteristics of snowfall in NJ, which improves our understanding of global snowfall microphysics and constitutes useful reference data for evaluating and verifying numerical simulations. The $\rho_s - D$ and $v - D$ relationships derived herein can be used as references for SR retrieval over East China. Dual-polarization radar observations should be used in the future research for hydrometeor classification of snowfall events, and to resolve the vertical structure of snowfall processes and further improve the performance of snowfall estimators.

REFERENCES

[1] S. Y. Matrosov, "A dual-wavelength radar method to measure snowfall rate," *J. Appl. Meteorol.*, vol. 37, no. 11, pp. 1510–1521, Nov. 1998.

[2] S. Y. Matrosov, C. Campbell, D. Kingsmill, and E. Sukovich, "Assessing snowfall rates from X-Band radar reflectivity measurements," *J. Atmos. Ocean. Technol.*, vol. 26, no. 11, pp. 2324–2339, Nov. 2009.

[3] Y. Fujiyoshi, T. Endoh, T. Yamada, K. Tsuboki, Y. Tachibana, and G. Wakahama, "Determination of aZ-RRelationship for snowfall using a radar and high sensitivity snow gauges," *J. Appl. Meteorol.*, vol. 29, no. 2, pp. 147–152, Feb. 1990.

[4] S. Y. Matrosov, "Radar reflectivity in snowfall," *IEEE Trans. Geosci. Remote Sens.*, vol. 30, no. 3, pp. 454–461, May 1992.

[5] E. A. Brandes, K. Ikeda, G. Thompson, and M. Schönhuber, "Aggregate terminal Velocity/Temperature relations," *J. Appl. Meteorol. Climatol.*, vol. 47, no. 10, pp. 2729–2736, Oct. 2008.

[6] A. Kruger and W. F. Krajewski, "Two-dimensional video disdrometer: A description," *J. Atmos. Ocean. Technol.*, vol. 19, no. 5, pp. 602–617, May 2002.

[7] M. Schoenhuber, G. Lammer, and W. L. Randeu, "The 2D-video-disdrometer," in *Precipitation: Advances in Measurement, Estimation and Prediction*. Berlin, Germany: Springer-Verlag, 2008, pp. 3–29.

[8] L. Wen, K. Zhao, G. Zhang, S. Liu, and G. Chen, "Impacts of instrument limitations on estimated raindrop size distribution, radar parameters, and model microphysics during mei-yu season in east China," *J. Atmos. Ocean. Technol.*, vol. 34, no. 5, pp. 1021–1037, May 2017.

[9] G. Zhang, M. Xue, Q. Cao, and D. Dawson, "Diagnosing the intercept parameter for exponential raindrop size distribution based on video disdrometer observations: Model development," *J. Appl. Meteorol. Climatol.*, vol. 47, no. 11, pp. 2983–2992, Nov. 2008.

[10] E. A. Brandes, K. Ikeda, G. Zhang, M. Schönhuber, and R. M. Rasmussen, "A statistical and physical description of hydrometeor distributions in colorado snowstorms using a video disdrometer," *J. Appl. Meteorol. Climatol.*, vol. 46, no. 5, pp. 634–650, May 2007.

[11] G.-J. Huang, V. N. Bringi, R. Cifelli, D. Hudak, and W. A. Petersen, "A methodology to derive radar reflectivity–liquid equivalent snow rate relations using C-Band radar and a 2D video disdrometer," *J. Atmos. Ocean. Technol.*, vol. 27, no. 4, pp. 637–651, Apr. 2010.

[12] G. Zhang, S. Luchs, A. Ryzhkov, M. Xue, L. Ryzhkova, and Q. Cao, "Winter precipitation microphysics characterized by polarimetric radar and video disdrometer observations in central oklahoma," *J. Appl. Meteorol. Climatol.*, vol. 50, no. 7, pp. 1558–1570, Jul. 2011.

[13] G.-J. Huang, V. N. Bringi, D. Moisseev, W. A. Petersen, L. Bliven, and D. Hudak, "Use of 2D-video disdrometer to derive mean density–size and Ze–SR relations: Four snow cases from the light precipitation validation experiment," *Atmos. Res.*, vol. 153, pp. 34–48, Feb. 2015.

[14] H. P. Böhm, "A general equation for the terminal fall speed of solid hydrometeors," *J. Atmos. Sci.*, vol. 46, no. 15, pp. 2419–2427, Aug. 1989.

[15] B. Sevruk, M. Ondrás, and B. Chvíla, "The WMO precipitation measurement intercomparisons," *Atmos. Res.*, vol. 92, no. 3, pp. 376–380, May 2009.

[16] B. E. Goodison, P. Y. T. Louie, and D. Yang, *WMO Solid Precipitation Measurement Intercom parison*. Geneva, Switzerland: World Meteorological Organization, 1998, pp. 255–262.

[17] R. Rasmussen *et al.*, "Weather support to deicing decision making (WSDDM): A winter weather nowcasting system," *Bull. Amer. Meteorol. Soc.*, vol. 82, no. 4, pp. 579–595, Apr. 2001.

[18] T. J. Schuur, H.-S. Park, A. V. Ryzhkov, and H. D. Reeves, "Classification of precipitation types during transitional winter weather using the RUC model and polarimetric radar retrievals," *J. Appl. Meteorol. Climatol.*, vol. 51, no. 4, pp. 763–779, Apr. 2012.

[19] R. E. Stewart, J. M. Thériault, and W. Henson, "On the characteristics of and processes producing winter precipitation types near 0°C," *Bull. Amer. Meteorol. Soc.*, vol. 96, no. 4, pp. 623–639, Apr. 2015.

[20] J. Zhang *et al.*, "Multi-radar multi-sensor (MRMS) quantitative precipitation estimation: Initial operating capabilities," *Bull. Amer. Meteorol.. Soc.*, vol. 97, no. 4, pp. 621–638, Apr. 2016.

[21] R. Stull, "Wet-bulb temperature from relative humidity and air temperature," *J. Appl. Meteorol. Climatol.*, vol. 50, no. 11, pp. 2267–2269, Nov. 2011.

[22] E. A. Brandes, G. Zhang, and J. Vivekanandan, "Experiments in rainfall estimation with a polarimetric radar in a subtropical environment," *J. Appl. Meteorol.*, vol. 41, no. 6, pp. 674–685, Jun. 2002.

[23] J.-E. Lee, S.-H. Jung, H.-M. Park, S. Kwon, P.-L. Lin, and G. Lee, "Classification of precipitation types using fall velocity-diameter relationships from 2D-video distrometer measurements," *Adv. Atmos. Sci.*, vol. 32, no. 9, pp. 1277–1290, Sep. 2015.

[24] J. D. Locatelli and P. V. Hobbs, "Fall speeds and masses of solid precipitation particles," *J. Geophys. Res.*, vol. 79, no. 15, pp. 2185–2197, May 1974.

[25] P. Bukoväiä, A. Ryzhkov, D. Zrnić, and G. Zhang, "Polarimetric radar relations for quantification of snow based on disdrometer data," *J. Appl. Meteorol. Climatol.*, vol. 57, no. 1, pp. 103–120, Jan. 2018.

[26] C. W. Ulbrich, "Natural variations in the analytical form of the raindrop size distribution," *J. Climate Appl. Meteorol.*, vol. 22, no. 10, pp. 1764–1775, Oct. 1983.

[27] A. J. Heymsfield *et al.*, "Observations and parameterizations of particle size distributions in deep tropical cirrus and stratiform precipitating clouds: Results from *in situ* observations in TRMM field campaigns," *J. Atmos. Sci.*, vol. 59, no. 24, pp. 3457–3491, Dec. 2002.

[28] A. J. Heymsfield, A. Bansemer, C. Schmitt, C. Twohy, and M. R. Poellot, "Effective ice particle densities derived from aircraft data," *J. Atmos. Sci.*, vol. 61, no. 9, pp. 982–1003, May 2004.

[29] L. Liao, R. Meneghini, T. Iguchi, and A. Detwiler, "Use of dual-wavelength radar for snow parameter estimates," *J. Atmos. Ocean. Technol.*, vol. 22, no. 10, pp. 1494–1506, Oct. 2005.

[30] J. Yang and H. Lei, "*in situ* observations of snow particle size distributions over a cold frontal rainband within an extratropical cyclone," *Asia–Pacific J. Atmos. Sci.*, vol. 52, no. 1, pp. 51–62, Feb. 2016.

[31] G. Zhao, R. Chu, T. Zhang, and W. Jia, "Analysis of the characteristics of snow drop size distribution in the Qilian mountains," *Sci. Cold Arid Regions*, vol. 2, no. 5, pp. 419–426, 2010.

[32] J. Vivekanandan, G. Zhang, and E. Brandes, "Polarimetric radar estimators based on a constrained gamma drop size distribution model," *J. Appl. Meteorol.*, vol. 43, no. 2, pp. 217–230, Feb. 2004.

[33] E. W. Holroyd, III, "The meso- and microscale structure of great lakes snowstorm bands: A synthesis of ground measurements, radar data, and satellite observations," Ph.D. dissertation, State Univ. New York Albany, Albany, NY, USA, 1971.

[34] F. Fabry and W. Szyrmer, "Modeling of the melting layer. Part II: Electromagnetic," *J. Atmos. Sci.*, vol. 56, no. 20, pp. 3593–3600, Oct. 1999.

[35] M. Krystek and M. Anton, "A weighted total least-squares algorithm for fitting a straight line," *Meas. Sci. Technol.*, vol. 18, no. 11, pp. 3438–3442, Nov. 2007.

[36] D. Atlas, M. Kerker, and W. Hitschfeld, "Scattering and attenuation by non-spherical atmospheric particles," *J. Atmos. Terr. Phys.*, vol. 3, no. 2, pp. 108–119, Feb. 1953.

[37] A. Sihvola, *Electromagnetic Mixing Formulas and Applications*. London, U.K.: IEE, 1999, p. 284.

[38] P. L. Smith, "Equivalent radar reflectivity factors for snow and ice particles," *J. Climate Appl. Meteorol.*, vol. 23, no. 8, pp. 1258–1260, Aug. 1984.

[39] R. C. Weast, *Handbook of Chemistry and Physics*. Boca Raton, FL, USA: CRC Press, 1977.

[40] E. Barthazy and R. Schefold, "Fall velocity of snowflakes of different riming degree and crystal types," *Atmos. Res.*, vol. 82, nos. 1–2, pp. 391–398, Nov. 2006.

[41] A. Heymsfield, "Ice crystal terminal velocities," *J. Atmos. Sci.*, vol. 29, no. 7, pp. 1348–1357, Oct. 1972.

[42] M. P. Bailey and J. Hallett, "A comprehensive habit diagram for atmospheric ice crystals: Confirmation from the laboratory, AIRS II, and other field studies," *J. Atmos. Sci.*, vol. 66, no. 9, pp. 2888–2899, Sep. 2009.

[43] K. L. S. Gunn and J. S. Marshall, "The distribution with size of aggregate snowflakes," *J. Meteorol.*, vol. 15, no. 5, pp. 452–461, Oct. 1958.

[44] L. Wen *et al.*, "Statistical characteristics of raindrop size distributions observed in east China during the asian summer monsoon season using 2-D video disdrometer and micro rain radar data," *J. Geophys. Res., Atmos.*, vol. 121, no. 5, pp. 2265–2282, Mar. 2016.

Ranting Tao received the B.S. degree in meteorology from the Chengdu University of Informational Technology, Chengdu, China, in 2017. She is currently pursuing the M.S. degree in meteorology with Nanjing University, Nanjing, China.

Her research interests include the study on microphysical characteristics of winter precipitation using disdrometer and polarimetric radar.

Kun Zhao received the B.S. degree in atmospheric physics and atmospheric environment and the Ph.D. degree in meteorology from Nanjing University, Nanjing, China, in 1998 and 2004, respectively.

After that, he joined the School of Atmospheric Sciences, Nanjing University, as a Faculty Member, where he is currently a Professor. From 2005 to 2006, he visited the P3 Mesoscale Meteorology Research Laboratory, National Taiwan University, Taipei, Taiwan, as a Post-Doctoral Researcher. From 2008 to 2010, he worked as a Visiting Scholar with the Center for Analysis and Prediction of Storms, Oklahoma University, Norman, OK, USA. He is currently also the Director of the Joint Center for Atmospheric Radar Research sponsored by the China Meteorological Administration and Nanjing University, Beijing, China. His research interests include the radar observation of severe convective storm and tropical cyclone, cloud and precipitation microphysics, radar data assimilation, and nowcasting.

Hao Huang received the B.S. degree and the Ph.D. degree in meteorology from Nanjing University, Nanjing, China, in 2011 and 2018, respectively.

From 2011 to 2013, he was a Weather Forecaster with Bengbu Meteorological Bureau, Bengbu, China. In 2015 and 2017, he was a Visiting Scholar with the Advanced Radar Research Center, The University of Oklahoma, Norman, OK, USA. He is currently a Research Associate with the School of Atmospheric Sciences, Nanjing University. His main research interests include the study of precipitation microphysics using radar and satellite data, radar quantitative precipitation estimation and forecasting, and the application of artificial intelligence algorithms in radar meteorology.

Long Wen received the B.S. and M.S. degrees in meteorology from Nanjing University, Nanjing, China, in 2011 and 2016, respectively.

Since 2011, he has been an Assistant Engineer of radar meteorology with the Xichang Satellite Launch Center (XSLC), Xichang, China. His research interests include remote sensing theory and technology for geophysical applications, and applying disdrometer and polarimetric radar observations to analyze precipitation microphysics and improve quantitative precipitation estimation.

Guifu Zhang (Senior Member, IEEE) received the B.S. degree in physics from Anhui University, Hefei, China, in 1982, the M.S. degree in radio physics from Wuhan University, Wuhan, China, in 1985, and the Ph.D. degree in electrical engineering from the University of Washington, Seattle, WA, USA, in 1998.

From 1985 to 1993, he was an Assistant Professor and an Associate Professor with the Space Physics Department, Wuhan University. In 1989, he worked as a Visiting Scholar with the Communication Research Laboratory, Tokyo, Japan. From 1993 to 1998, he studied and worked with the Department of Electrical Engineering, University of Washington, where he was first a Visiting Scientist and later a Ph.D. Student. From 1998 to 2005, he was a Scientist with the National Center for Atmospheric Research (NCAR), Boulder, CO, USA. In 2005, he joined the School of Meteorology, The University of Oklahoma, Norman, OK, USA, where he is currently a Professor. He formulated theories of weather radar interferometry and phased array radar polarimetry. He led the development of advanced signal processing algorithm to improve weather radar data quality and the polarimetric radar data simulators to bridge the gap between radar meteorology and numerical weather prediction. Among his current projects, he is working on topics such as the optimal use of polarimetric radar data (PRD) in quantitative precipitation estimation (QPE) and quantitative precipitation forecast (QPF) and the research and development of polarimetric phased array radars for weather measurements and multimission capability. He has authored *Weather Radar Polarimetry* and over 100 journal publications for his research work in radar theory/technology, signal processing, and applications, and filed over ten intellectual property disclosures.

Dr. Zhang has received four U.S. patent awards and several research and excellent paper awards.

Ang Zhou received the B.S. degree in meteorology from Nanjing University, Nanjing, China, in 2017, where he is currently pursuing the Ph.D. degree.

His main research interest is the microphysical processes of mesoscale severe weather using polarimetric radar observations.

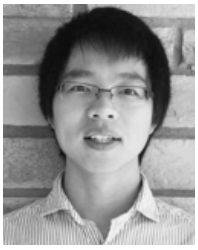

Haonan Chen (Member, IEEE) received the bachelor's degree from the Chongqing University of Posts and Telecommunications, Chongqing, China, in 2010, and the M.S. and Ph.D. degrees from Colorado State University (CSU), Fort Collins, CO, USA, in 2013 and 2017, respectively, all in electrical engineering.

He has been working with the Physical Sciences Division (PSD), NOAA Earth System Research Laboratory, Boulder, CO, since 2012, first as a Research Student, then a National Research Council Research Associate, and currently a Radar, Satellite, and Precipitation Scientist through the Cooperative Institute for Research in the Atmosphere (CIRA), Fort Collins. He is also an Affiliate Faculty Member with the Department of Electrical and Computer Engineering, CSU. His research interest is mainly to advance the understanding of the physical sciences in the hydrometeorological processes using remote sensing technologies. He specializes in radar systems and networking, precipitation classification and estimation with polarimetric radar measurements, and multiscale radar and satellite data fusion.

Dr. Chen serves as an Associate Editor for the *Journal of Atmospheric and Oceanic Technology* and *URSI Radio Science Bulletin*, and a Guest Editor for *Remote Sensing*.